Evolution of microstructure, texture and grain boundary character distribution of potassium doped tungsten fibers annealed at variable temperatures

IOP Conf. Series: Journal of Physics: Conf. Series **1270** (2019) 012038 doi:10.1088/1742-6596/1270/1/012038

Evolution of microstructure, texture and grain boundary character distribution of potassium doped tungsten fibers annealed at variable temperatures

L Tanure[1, 2*], D Terentyev[3], J Riesch[4] and K Verbeken[1]

[1]*Department of Materials, Textiles and Chemical Engineering, Ghent University (UGent), Technologiepark 46, B-9052 Ghent, Belgium*
[2]*Dutch Institute for Fundamental Energy Research, DIFFER, De Zaale 20, 5612 AJ Eindhoven, The Netherlands*
[3]*Nuclear Materials Science Institute, SCK.CEN, Boeretang 200, 2400 Mol, Belgium*
[4]*Max-Planck-Institut für Plasmaphysik, Garching, Germany*

E-Mail: leandro.tanure@ugent.be

Abstract: The effect of the annealing temperature on the microstructure and grain boundary character distribution of potassium doped tungsten fibers made of drawn wire was investigated by Electron Backscatter Diffraction. Samples, with a diameter of 148.7 µm, in the as-received condition and annealed at 1300, 1600, 1900, 2100 and 2300 °C were analyzed at the center of the transversal sections. Up to 1900 °C, a uniform microstructural coarsening and primary recrystallization followed by normal grain growth was observed. Between 1900 and 2100 °C abnormal grain growth took place. The strong texture (<110> parallel to the drawing axis) remained present in all conditions. With increasing the annealing temperature, the low angle grain boundary fraction increased at the expense of high angle grain boundaries while the amount of coincidence site lattice boundaries reached its maximum at 1600 °C. At this temperature, the most resistant configuration of triple junctions against intergranular crack propagation was obtained.

1. Introduction

Recently, several studies have been carried out to evaluate the use of tungsten (W) based materials as plasma facing components for future nuclear fusion reactors (i. e. ITER and DEMO) [1]. Despite its suitability for such application, due to its refractory nature, low sputtering erosion, good thermal conductivity, low tritium retention and high strength, W possesses intrinsic brittleness below the so-called ductile-to-brittle transition temperature and can be even further embrittled by neutron irradiation and overheating [2]. A possible way to mitigate these issues is to reinforce W with W fibers, made of W wires doped with potassium to improve their temperature stability. The fiber-reinforcement promotes a toughening mechanism analogous to that of a fiber-reinforced ceramic matrix composite which relies on energy dissipation by controlled mechanisms at the fiber/matrix interfaces [2]. Additionally, the dopant effect of potassium results in pinning of the grain boundaries as such suppressing recrystallization [3].

Given the concept of reinforcement, the behavior of the composite will be very much determined by the properties of the W-fibers [4]. Given that plasma-facing components will be subjected to

significant heat loads, the resistance of the fibers against the high temperature annealing is important aspect to be addressed and has been extensively studied in the past years [5–11]. Potassium has already proven to restrict grain boundary mobility and keep ductile fracture even after annealing at very high temperatures (1600-1900 °C), since the decrease in fracture toughness is not as pronounced as in pure W-fibers, but a better understanding on the role of triple junctions is still missing. The goal of the present study is to assess the effect of the annealing temperature on microstructure, texture, grain boundary character distribution and evolution of the triple junctions of K-doped W-fiber via Electron Backscatter Diffraction (EBSD) analysis.

2. Materials and Methods

Drawn potassium doped wires (60 – 75 ppm K), with a diameter of 148.7 ± 0.2 µm, were provided by OSRAM GmbH, Schwabmünchen. Segments of 100 mm long were annealed in a tube furnace, under hydrogen atmosphere, at 1300, 1600, 1900, 2100 and 2300 °C for 30 minutes [6]. Samples with 5 mm length were cut, mounted, grinded and polished up to 1 µm diamond paste suspension following the standard metallographic procedures. An additional step of polishing with OP-U suspension was required for EBSD analysis. The specimens were scanned at the center of the transversal cross-section using a Field Emission Gun Quanta-450 FEI Scanning Electron Microscope in areas of 40x40 µm^2 with step-sizes of 0.05 and 0.10 µm. Image post-processing were carried out with the OIM® Analysis software. The size of the areas were chosen taking into account a balance between the number of grains (as much as possible) and the effect that the edges of a rectangular area could have on the analysis of a round cross-section.

3. Results and Discussion

Figures 1 (a-f) show Inverse Pole Figure (IPF) maps overlapped with Image Quality (IQ) maps of the K-doped W-fibers in all conditions. Figures 1(g) and (h) display the zoomed-in IQ maps (in smaller areas) of the samples in the as-received and annealed at 1300 °C conditions.

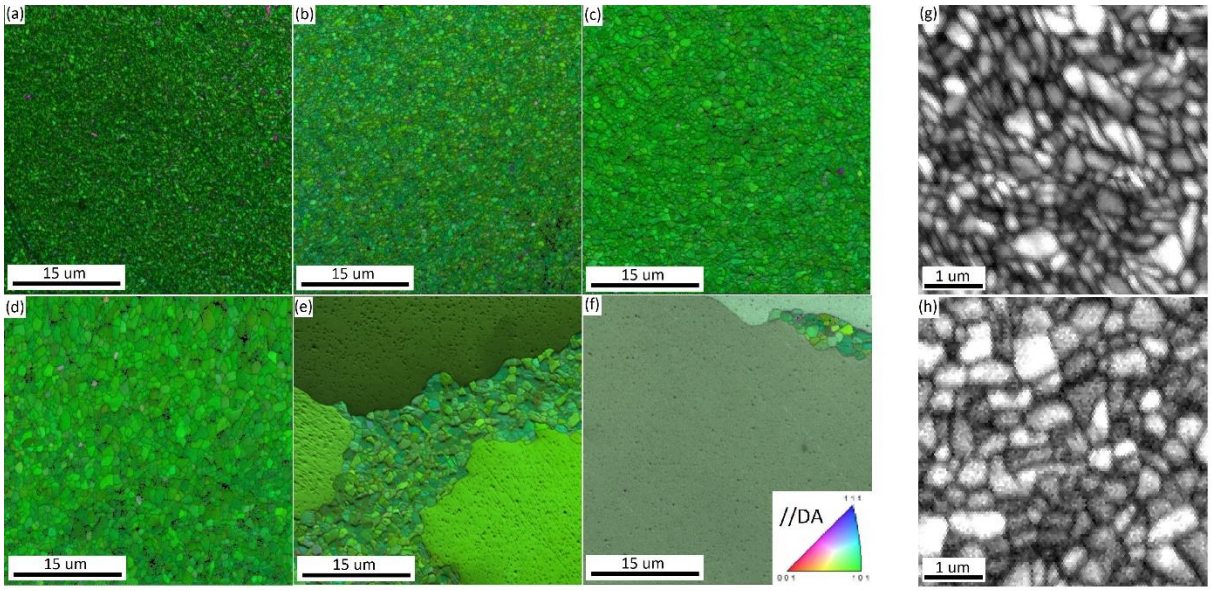

Figure 1. Inverse Pole Figure overlapped with Image Quality maps of K-doped tungsten samples in the (a) as-received condition and annealed at (b) 1300 °C, (c) 1600 °C, (d) 1900 °C, (e) 2100 °C and (f) 2300 °C. Color code with respect to the Drawing Axis (DA). (g) and (h) detail of the IQ maps of the as-received and annealed at 1300 °C conditions, respectively.

Up to 1900 °C, i.e. figures 1(a), (b), (c) and (d), one can notice a uniform and progressive change in the grain size. From 2100 °C on, figures 1(e) and (f), abnormal grain growth takes place and the maps are dominated by a few very large grains. Therefore, these conditions were excluded from further analysis due to the dominance of these grains which implies a lack of statistics in the analyzed parameters (texture, grain boundary character distribution and average grain size).

The average grain sizes, calculated by the software, are 0.45 ± 0.30, 0.63 ± 0.37, 0.90 ± 0.59 and 1.25 ± 0.71 μm for the as-received and annealed at 1300, 1600 and 1900 °C conditions, respectively. Despite the large standard deviation, a gradual and continuous growth can be noticed. These samples present unimodal grain size distribution and no exaggerated grain growth was observed.

In studies carried out by Jansen [3] and, recently, by Zhao et al. [8] on microstructure of W-fibers after different heat treatments, recrystallization was ascribed to small morphological changes in the transversal cross-section. According to Zhao, when a curly shape, also referred as Van Gogh sky structure (due to the resemblance with the painting style of the famous painter), is no longer observed and, according to Jansen, when ribbon-shaped fiber-crystals transform quickly into stem-like crystals with polygonal cross-section, recrystallization has taken place. Figures 1(g) and (h) show IQ maps of a 5 x 5 μm^2 area where clear differences between microstructures of the as-received and annealed at 1300 °C conditions can be seen. Grains slightly larger of the annealed condition replace the smaller grains of the as-received condition suggesting a recrystallized microstructure.

The grain growth is kept under control up to 1900 °C. This behavior agrees with observations made by Jansen and by Terentyev et al. [5] on K-doped W-fibers where abnormal grain growth occurred only above 2000 °C. Annealing at such high temperature is required to achieve the secondary recrystallization stage thanks to the very effective dragging of the grain boundary migration by the potassium dopant. Potassium remains entrapped inside some residual pores that are stretched along the axis direction during wire drawing forming narrow ellipsoids that break up into a single row of spherical and nano-sized bubbles upon annealing [12].

The samples presented a very strong <110> // DA texture as can be seen in both figure 1, due to the dominance of the green color on the IPF maps, and figure 2 with peaks of 15.7, 16.7, 17.0 and 16.6 times random for the as-received, and annealed at 1300, 1600 and 1900 °C conditions, respectively. This texture could be expected for body-centered cubic materials that underwent wire drawing [13]. Therefore, the annealing temperature did not have a significant effect on texture intensities since all conditions have similar texture intensities.

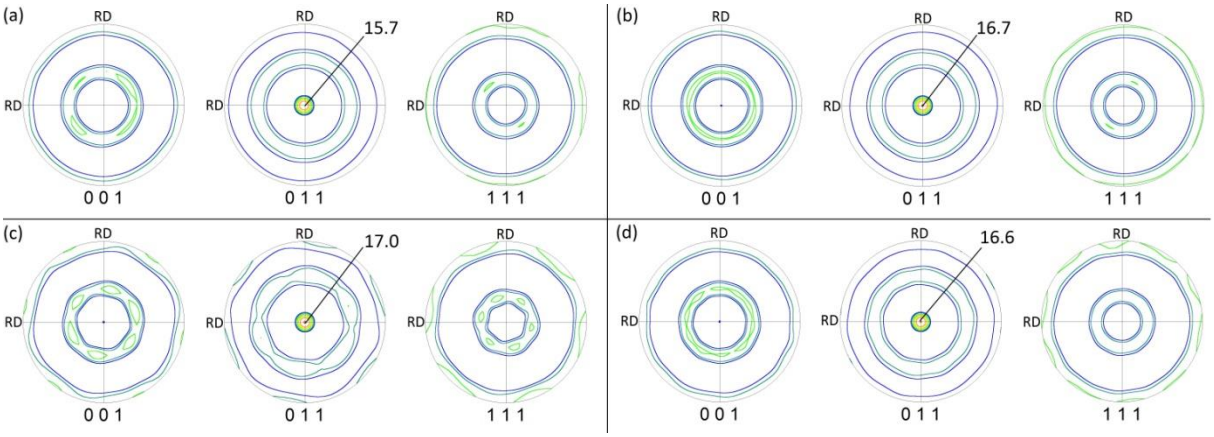

Figure 2. Pole figures of the samples with unimodal grain size distribution in the (a) as-received and annealed at (b) 1300, (c) 1600 and (d) 1900 °C conditions. DA perpendicular to the paper. RD: radial direction. Intensity levels: 1-2-4-6-8-11-16 times random.

The analysis of the Coincidence Site Lattices (CSL – from Σ3 to Σ29) followed the Brandon's Criterion for a maximum permissible deviation given by $\Delta\theta=\theta_0(\Sigma)^{-n}$ where θ=15 and n=0.5. By raising

the annealing temperature the number fraction of low angle grain boundaries (LAGBs – misorientation angles between 2 and 15°) has gradually increased from 0.292 to 0.345, 0.375 and 0.394 for the as-received and annealed at 1300, 1600 and 1900 °C conditions, respectively, whereas the fraction of high angle grain boundaries (HAGBs – misorientation angles >15°) has reduced from 0.478 to 0.371, 0.341 and 0.357, respectively, for the same annealing conditions. The CSL fraction is 0.229 (as-received), 0.283 (annealed at 1300 °C), 0.284 (annealed at 1600 °C) and 0.249 (annealed at 1900 °C). This remarkable trend, expressed in the increase of LAGBs fraction at expense of HAGBs, as well as the large fraction of HAGBs in the as-received condition can be explained by the grain subdivision mechanism. It occurs when dislocation accumulation processes take place surrounding deformed crystallites during continuous deformation resulting in the increase of the misorientation angle. With the increase of annealing temperature, the reduction of HAGBs is ascribed to the strong texture developed during wire drawing (as shown in figure 2 and reported in [5,10]) that is responsible for the orientation pinning effect (when a growing grain meets a deformed crystallite with similar orientation causing the replacement of the mobile HAGB by a less mobile LAGB) [14].

Some studies have already pointed out that specific features of the materials such as stress corrosion crack propagation resistance can be enhanced with the increase of CSL boundary fraction due to particular properties related to the enhanced atomic diffusion or dislocation glide [15]. Figure 3(a) shows the distribution of the CSL clearly dominated by Σ3, Σ9, Σ11, Σ19a and Σ27a types. The same boundaries were also reported by Watanabe [16] and related to strong <110> texture in Fe-6.5%Si ribbons. The increase in Σ3 fraction at expense of both Σ9 and Σ27a is a well-known feature described in detail by the *"Σ3 regeneration model"* proposed by Randle in order to explain how the Σ3 boundary fraction can be enhanced in the network of low stacking-fault energy materials [17]. Although tungsten is a body-centered cubic metal with high stacking-fault energy, there is a slight similar but inconclusive trend observed in this work that Randle's prediction was followed.

The grain boundary connectivity has an important role regarding the control of a dominant fracture mode in polycrystalline materials, since triple junctions (TJ) can act as either a crack arrester or a crack assister (to accumulate stress concentration) depending on the distribution and interconnectivity of the boundaries prone to crack propagation[18]. Figure 3(b) shows the four types of TJs that can occur in a material, combinations of random boundaries (R) with special (S) CSL boundaries, i.e. 0-CSL (RRR), 1-CSL (RRS), 2-CSL (RSS) and 3-CSL (SSS), whereas figure 3(c) shows the TJ Distribution of the fibers with unimodal grain size distribution. If a TJ comprises at least 2-CSL (RSS) boundaries, the random boundary network connectivity will be broken, as well as the pathway to intergranular degradation. Therefore, the number of special CSL boundaries in a TJ provides an indication of failure resistance.

According to figure 3(c), up to 1600 °C, there is a reduction of RRR and RRS TJ types and an increase in both RSS and SSS (with the CSL fractions increase) which are critical components in predicting the breaking-up of the grain boundary network connectivity [19]. This behavior was observed and detailed by Fortier et al. [19] in aluminum and copper and can be explained based on the Σ3 regeneration model. When a Σ3 boundary interacts with another Σ3, the third boundary will probably be a Σ9 rather than a LAGB. If the interaction is between Σ3 and $\Sigma 3^n$, the third boundary will most likely be $\Sigma 3^{n-1}$ rather than a $\Sigma 3^{n+1}$. Both interactions reduce the availability of random boundaries at TJ, therefore, leading to an increase of TJ fractions where special boundaries are more abundant (RSS and SSS) at the expense of the other TJs types. Finally, for the sake of completeness, if the Σ3 interacts with a random boundary, the newly created boundary at the TJ will have four out of five degrees of freedom fixed. When this happens, this implies that the indices of the grain boundary plane must be affected [17].

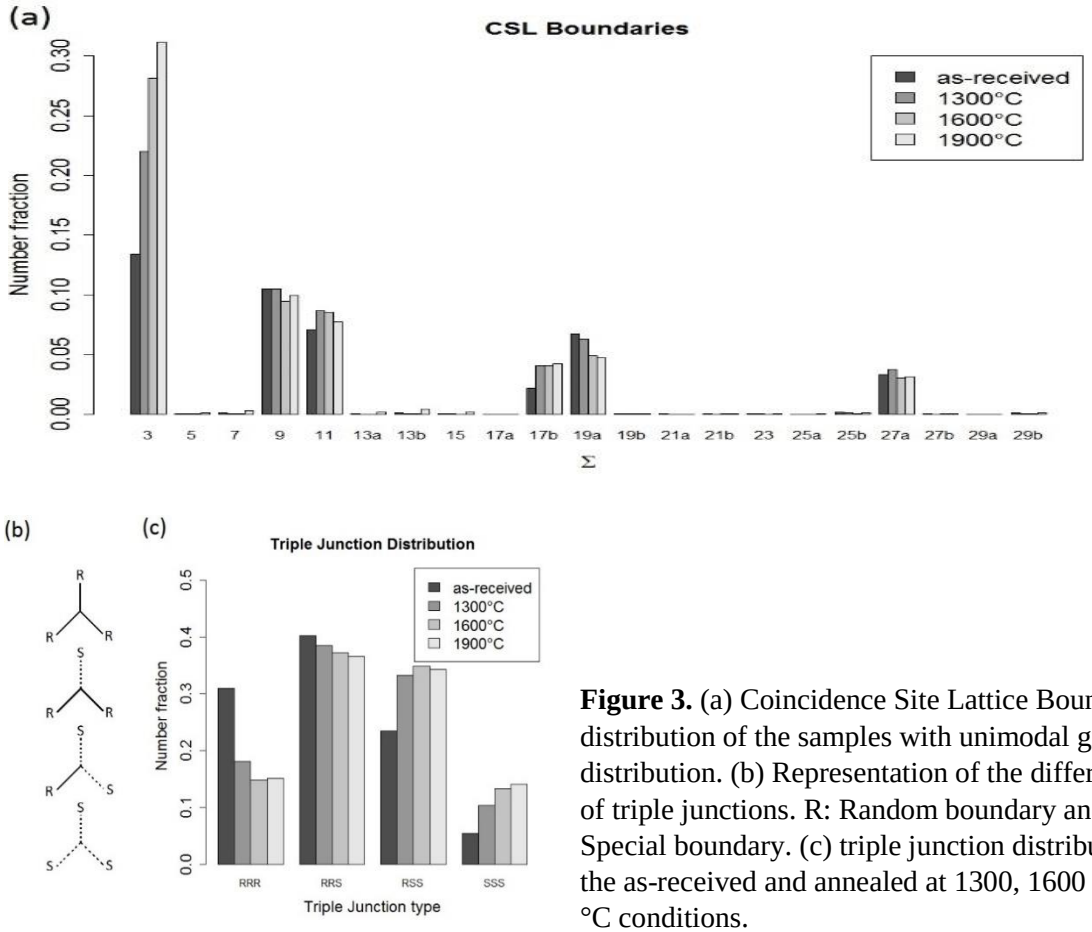

Figure 3. (a) Coincidence Site Lattice Boundaries distribution of the samples with unimodal grain size distribution. (b) Representation of the different types of triple junctions. R: Random boundary and S: Special boundary. (c) triple junction distributions of the as-received and annealed at 1300, 1600 and 1900 °C conditions.

Due to the large fraction of CSL boundaries in all conditions (around 0.25-0.30) the resistance of the microstructure must be assessed in terms of TJs since the connectivity of the grain boundaries plays a more important role on crack propagation than the CSL fraction itself [19]. For this evaluation, one should consider the distribution of TJs that comprise at least one boundary susceptible to cracking, therefore, the SSS type will be considered as non-active entity regarding crack propagation. If the ratio $f_{RSS}/(1-f_{SSS}) \geq 0.35$ (where f_{RSS} and f_{SSS} are the number fractions of TJs composed by two and three special boundaries, respectively) percolative paths in the microstructure, which could act as a crack assister, will be broken reducing the connectivity of random boundaries. This ratio of percolative-resistant TJs gives an estimate of the fraction of TJs capable of arresting a propagating crack [18] and are equal to 0.25, 0.37, 0.40 and 0.39 for the as-received and annealed at 1300, 1600 and 1900 °C conditions, respectively. Although these values are very close to each other, according to this evaluation, annealing promotes the increase of resistant TJ distribution regarding intergranular crack propagation indicating that another fracture mechanism could prevail. Depending on the TJ distribution, if an initially formed intergranular crack cannot continue to propagate because of meeting a resistant TJ, RSS, the crack proceeds as a mixture of intergranular and transgranular fracture. If there are no resistant TJs, the crack will propagate connecting random weak boundaries resulting in typical intergranular fracture showing severe brittleness. These results are consistent with our previous study where surface fracture analysis were carried out on tensile tested W-pure and K-doped fibers that were annealed in the same conditions [5]. The K-doped fibers were more resistant to intergranular fracture in comparison with W-pure fibers [7] due to the elongated grains that remained in the microstructure

up to 1900 °C. Future comparative studies on the effect of annealing temperature on TJ character of both W-pure and K-doped fibers will help to clarify the role of TJs on mechanical behavior.

4. Conclusions

The effect of annealing temperature on microstructure, texture, grain boundary character and triple junction character distributions of K-doped W-fibers was evaluated and discussed in terms of EBSD analysis. Primary recrystallization was observed at 1300 °C followed by normal grain growth up to 1900 °C. Secondary recrystallization took place between 1900 and 2100 °C confirming the strong effect of potassium on suppressing the abnormal grain growth. The annealing temperature did not impact the texture development that remained very strong, around 16 times random, with <110> components parallel to the Drawing Axis. As the annealing temperature increased, there was a reduction on HAGBs and an increase of LAGBs fractions. The fraction of CSL has increased up to 1600 °C and could be linked with the increase of percolation-resistant TJ fractions as well as the increase of TJs where 2 and 3 CSL boundaries were present (RSS and SSS).

Acknowledgement

This work has been carried out within the framework of Erasmus Mundus Fusion-DC and the EUROfusion Consortium. It has received funding from the Euratom research and training programme 2014-2018 and 2019-2020 under grant agreement No 633053. The views and opinions expressed herein do not necessarily reflect those of the European Commission.

References

[1] Hirai T, Escourbiac F, Barabash V, Durocher A, et al. 2015 *J. Nucl. Mater.* **463** 1248–51
[2] Riesch J, Aumann M, Coenen J W, et al. 2016 *Nucl. Mater. Energy* **9** 75–83
[3] Jansen H H R 1987 *Philips J. Res.* **42** 3–14
[4] Gietl H, Riesch J, Coenen J W, et al. 2017 *Fusion Eng. Des.* **124** 396–400
[5] Terentyev D, Tanure L, Bakaeva A, et al. 2019 *Int. J. Refract. Met. Hard Mater.* **81** 253–71
[6] Terentyev D, Van Renterghem W, Tanure L, et al. 2019 *Int. J. Refract. Met. Hard Mater.* **79** 204–16
[7] Terentyev D, Riesch J, Dubinko A, Khvan T and Zhurkin E E 2019 *Fusion Eng. Des.* 1–4
[8] Zhao P, Riesch J, Höschen T, et al. 2017 *Int. J. Refract. Met. Hard Mater.* **68** 29–40
[9] Riesch J, Han Y, Almanstötter J, et al. 2016 *Phys. Scr.* **T167** 14006
[10] Nikolić V, Riesch J and Pippan R 2018 *Mater. Sci. Eng. A* **737** 422–33
[11] Nikolić V, Riesch J, Pfeifenberger M J and Pippan R 2018 *Mater. Sci. Eng. A* **737** 434–47
[12] Horacsek O, Briant C L and Horacsek K 1997 *High Temp. Process.* **16** 15–27
[13] Engler O and Randle V 2010 *Introduction to Texture Analysis: Macrotexture, Microtexture and Orientation Mapping* (CRC Press Taylor & Francis Group)
[14] Hughes D A and Hansen N 1997 *Acta Mater.* **45** 3871–86
[15] Lehockey E M, Palumbo G, Lin P and Brennenstuhl A M 1997 On the relationship between grain boundary character distribution and intergranular corrosion *Scr. Mater.* **36** 1211–8
[16] Watanabe T, Fujii H, Oikawa H and Arai K I 1989 *Acta Metall.* **37** 941–52
[17] Randle V 2004 *Acta Mater.* **52** 4067–81
[18] King W E, Stolken J S, Kumar M and Schwartz A J 2000 *Electron Backscatter Diffraction in Materials Science* ed A J Schwartz, M Kumar and B L Adams (New York)
[19] Fortier P, Miller W a. and Aust K T 1997 *Acta Mater.* **45** 3459–67
[20] Randle V 2010 *Mater. Sci. Tech.* **26** 774-80